Theory and analysis of differentially-driven microstrip antennas

Zhang, Yue Ping; Wang, Jun Jun

2006

Zhang, Y. P., & Wang, J. J. (2006). Theory and analysis of differentially-driven microstrip antennas. IEEE Transactions on Antennas and Propagation, 54(4), 1092-1099.

https://hdl.handle.net/10356/91620

https://doi.org/10.1109/TAP.2006.872597

Theory and Analysis of Differentially-Driven Microstrip Antennas

Y. P. Zhang and J. J. Wang

***Abstract*—This paper studies differentially-driven microstrip antennas. The theory of microstrip antennas based on the improved cavity model is expanded to analyze the input impedance and radiation characteristics of the differentially-driven microstrip antennas. The differentially-driven microstrip antennas were fabricated. Their performances were experimentally verified. Results show that the occurrence of resonance for the differentially-driven microstrip antennas also depends on the ratio of the separation ξ of the dual feeds to the free-space wavelength λ_o. When the dual feeds are located far from each other $\xi/\lambda_o > 0.1$, the resonance occurs, and the input resistance at resonance is rather large. However, when the dual feeds are located near to each other $\xi/\lambda_o < 0.1$, the resonance does not occur, the input resistance is quite small, and the input impedance is inductive. Compared with single-ended microstrip antennas, the differentially-driven microstrip antennas have larger resonant resistance, similar co-polar radiation patterns, and lower cross-polar radiation component.**

***Index Terms*—Cavity model, input impedance, microstrip patch antenna, radiation pattern.**

I. Introduction

MICROSTRIP antennas have many unique and attractive properties—low in profile, light in weight, compact and conformable in structure, and easy to fabricate and to be integrated with solid-state devices [1]. Microstrip antennas have found wide applications in radio systems with single-ended signal operation. Recently, microstrip antennas can be seen for use in radio systems with differential signal operation as well [2]–[5]. For example, a differentially-driven microstrip antenna integrated with a push-pull power amplifier in Gallium Arsenide semiconductor technology is reported in [2]. The differentially-driven microstrip antenna acts also as an output balun, which makes the push-pull power amplifier more compact and efficient. A second differentially-driven microstrip antenna integrated with a push-pull power amplifier in complimentary metal oxide semiconductor technology is presented in [3]. The differentially-driven microstrip antenna takes full advantages of the standard surface-mounted ceramic ball grid array package; consequently, the system-level board space and the system-level assembly can be reduced and facilitated, respectively. A third differentially-driven microstrip antenna integrated with an oscillator including a buffer amplifier in Silicon Germanium semiconductor technology is proposed in [4]. The differentially-driven microstrip antenna introduces a virtual ground; accordingly, there is no need for connecting the ground of the solid-state devices and the ground plane of the antenna, the parasitic effect caused by interconnect is eliminated. Besides these differentially-driven microstrip antennas, a differential receiving microstrip antenna integrated with a differential low noise amplifier in Gallium Arsenide semiconductor technology is described in [5]. The differential receiving microstrip antenna acts also as an input balun, which offers a new possibility to build small, robust and cost-effective smart antenna arrays. The above works focus on integration with solid-state devices and indeed provide little information on the design of differential microstrip antennas. Furthermore, the state of the art single-chip and single-package solutions of radio systems call for differential antennas to reduce the bill of materials and to improve the receiver noise performance and transmitter power efficiency [6], [7]. In this paper we present a study of differentially-driven microstrip antennas. We describe the theory of differentially-driven microstrip antennas based on the improved cavity model in Section II. The improved cavity model offers both simplicity and physical insight. We validate the theory with experiments and HFSS simulations in Section III. We apply the validated theory to analyze the differentially-driven microstrip antennas to gain deep insight into the differential operation of the microstrip antennas in Section IV. Finally, we summarize the conclusions in Section V.

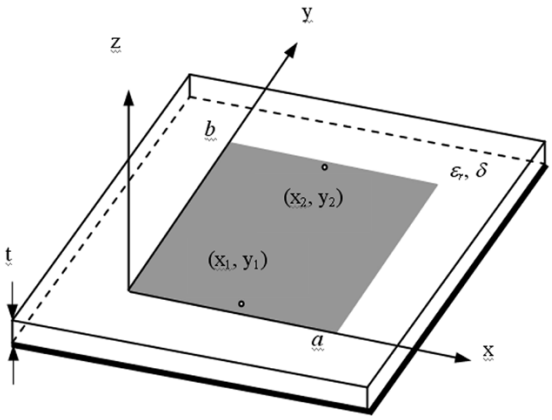

Fig. 1. Differentially-driven microstrip antenna.

II. Theory of Differentially-Driven Microstrip Antennas

A microstrip antenna and a coordinate system are illustrated in Fig. 1. The microstrip antenna that has dimensions a along x-axis and b along y-axis located on the surface of a grounded dielectric substrate with thickness t, dielectric constant ε_r, and

Manuscript received December 24, 2004; revised September 8, 2005.

The authors are with the Integrated Systems Research Laboratory, School of Electrical and Electronic Engineering, Nanyang Technological University, Singapore 639798, Singapore (e-mail: eypzhang@ntu.edu.sg).

Digital Object Identifier 10.1109/TAP.2006.872597

dielectric loss tangent δ is differentially driven at points (x_1, y_1) and (x_2, y_2).

The differentially-driven microstrip antenna can be treated as a two-port network. With reference to the ground plane, the driving point at (x_1, y_1) is defined as port 1 and the driving point at (x_2, y_2) as port 2. Using the Z parameters for ports 1 and 2; one can express the differential voltage V_d as

$$V_d = V_1 - V_2 = (Z_{11} - Z_{21})I_1 - (Z_{22} - Z_{12})I_2 \quad (1)$$

where V_1 and V_2 are the driving point voltages and I_1 and I_2 are the driving point currents of ports 1 and 2, respectively. Since for the differentially-driven microstrip antenna

$$I_1 = -I_2 = I. \quad (2)$$

Equation (1) simplifies to

$$Z_d = \frac{V_d}{I} = 2(Z_{11} - Z_{21}) = 2(Z_{22} - Z_{12}) \quad (3)$$

where Z_d is the input impedance of the differentially-driven microstrip antenna. The value of Z_d is required in the design of matching network between the differentially-driven microstrip antenna and the differential active circuitry in a radio system. The Z parameters for the microstrip antenna shown in Fig. 1 are calculated using the improved cavity model as follows [8]:

$$Z_{11} = j\omega\mu_o t \sum_{m,n=0}^{\infty} \frac{\phi_{mn}^2(x_1, y_1) j_o^2\left(\frac{m\pi d_e}{2a_e}\right)}{k_{mn}^2 - k_e^2} \quad (4)$$

$$Z_{12} = j\omega\mu_o t \sum_{m,n=0}^{\infty} \frac{\phi_{mn}(x_1, y_1)\phi_{mn}(x_2, y_2) j_o^2\left(\frac{m\pi d_e}{2a_e}\right)}{k_{mn}^2 - k_e^2} \quad (5)$$

where ω is angular frequency, μ_o is the permeability of vacuum, d_e is the effective width of a uniform strip of z directed source current of one amp

$$k_e^2 = \varepsilon_r(1 - j\delta_e)k_o^2 \quad (6)$$

$$k_o = \omega/v \quad (7)$$

$$k_{mn}^2 = (m\pi/a_e)^2 + (n\pi/b_e)^2 \quad (8)$$

$$j_o(x) = \sin(x)/x \quad (9)$$

$$\phi_{mn}(x, y) = \sqrt{\varepsilon_{0m}\varepsilon_{0n}/a_e b_e}\cos(m\pi x/a_e)\cos(n\pi y/b_e) \quad (10)$$

where $\varepsilon_{0m} = 1$ for $m = 0$ and 2 for $m \neq 0, m$ and n are the mode indices in the x and y directions, respectively, δ_e is the effective loss tangent, v is the speed of light, a_e and b_e are the effective dimensions, taking into account the fringing fields at the edge of the microstrip patch. Similarly, Z_{21} and Z_{22} can be computed. a_e may be approximated as follows [9]:

$$a_e = a + \left(\frac{b_{\text{eq}} - b}{2}\right)\frac{\varepsilon_e(b) + 0.3}{\varepsilon_e(b) - 0.258} \quad (11)$$

where $\varepsilon_e(b)$ is the effective dielectric constant and b_{eq} is the equivalent width calculated from the planar waveguide model. $\varepsilon_e(b)$ can be written as

$$\varepsilon_e(b) = \frac{\varepsilon_r + 1}{2} + \frac{\varepsilon_r - 1}{2}\left(1 + 10\frac{t}{b}\right)^{-1/2} \quad (12)$$

and b_{eq} as

$$b_{\text{eq}} = \frac{120\pi t}{Z(b)\sqrt{\varepsilon_e(b)}} \quad (13)$$

where $Z(b)$, the impedance of a microstrip line of width b and thickness t, is given by

$$Z(b) = \frac{60\pi}{\sqrt{\varepsilon_r}}\left\{\begin{array}{c}\frac{b}{2t} + 0.441 + 0.082\left[\frac{\varepsilon_r - 1}{\varepsilon_r^2}\right] \\ + \frac{(\varepsilon_r + 1)}{2\pi\varepsilon_r}\left[1.415 + Ln\left(\frac{b}{2t} + 0.94\right)\right]\end{array}\right\}^{-1}. \quad (14)$$

Similarly, b_e can be calculated by replacing $a, b_{\text{eq}}, b, Z(b)$, and $\varepsilon_e(b)$ in (11)–(14) with $b, a_{\text{eq}}, a, Z(a)$, and $\varepsilon_e(a)$, respectively.

Next, let us examine the radiation characteristics of the differentially-driven microstrip antenna. It is known that the radiation of the microstrip antenna originates from two slots and each slot can be thought of as radiating the same field as a magnetic dipole with a magnetic current of

$$M = 2\hat{n} \times \hat{z}E_z \quad (15)$$

where the factor of 2 comes from the image of the magnetic current in the ground plane, $\hat{n}$ is the outward normal to the magnetic wall, $\hat{z}$ is the unit vector in the z-direction, and E_z is the z component of electric field in the cavity region. For the differentially-driven microstrip antenna, E_z can be written as

$$E_z = j\mu_o \sum_{m,n=0}^{\infty} I\frac{\phi_{mn}(x, y)}{k_e^2 - k_{mn}^2} j_o\left(\frac{m\pi d_e}{2a_e}\right)\left[\begin{array}{c}\phi_{mn}(x_1, y_1) \\ -\phi_{mn}(x_2, y_2)\end{array}\right]. \quad (16)$$

where I is the source current of one amp in our calculation. Equation (16) reveals that the differentially-driven microstrip antenna introduces the cancellation mechanism, which can be explored to suppress some higher-order modes to reduce the cross polarization radiation. The electric vector potential of M is given by

$$F(r) = \frac{\varepsilon_o}{4\pi}\int \frac{M(r')}{|r - r'|}\exp(-jk_o|r - r'|)dl(r') \quad (17)$$

where ε_o is the permittivity of vacuum and integration is over the perimeter of the patch. The far field radiation components at a point $P(r, \theta, \phi)$ can be expressed as

$$E_\theta = j\omega\eta_o t(-F_x\sin\phi + F_y\cos\phi) \quad (18)$$

$$E_\phi = -j\omega\eta_o t(F_x\cos\theta\cos\phi + F_y\cos\theta\sin\phi) \quad (19)$$

where $\eta_o = 377\ \Omega$.

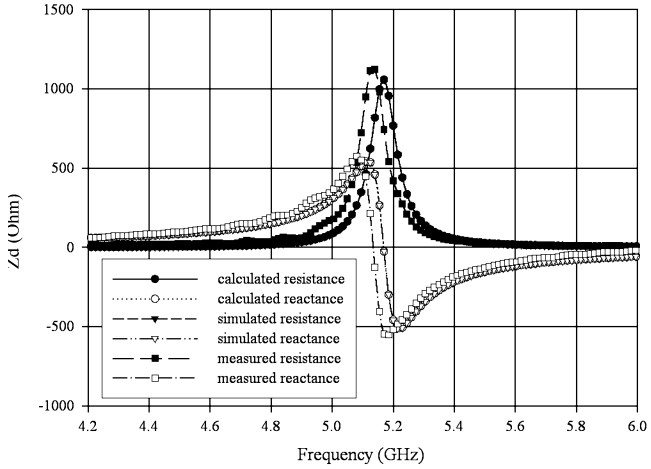

Fig. 2. Input impedance versus frequency of the differentially-driven microstrip antenna.

In the implementation of the improved cavity model, the determination of the effective loss tangent δ_e is critical. This is because the effective loss tangent δ_e is introduced to account for the total losses in the cavity. If the dielectric substrate is thin so that surface wave loss can be negligible, δ_e is given by

$$\delta_e = \frac{P_r + P_d + P_c}{2\omega W_e} \tag{20}$$

where P_r, P_d, and P_c are radiation, dielectric, and conductor losses, respectively, and W_e is electric energy stored in the cavity under the patch at resonance. The effective loss tangent δ_e can be written, near the resonant frequency, according to (20), as [10]

$$\delta_e = \frac{P_r}{2\omega W_e} + \delta + \frac{s}{t} \tag{21}$$

where $s = 0.029\sqrt{\lambda_o/\sigma}$ is the skin depth in the metal cladding with conductivity σ (with units of Siemens per meter). The radiation loss by the space wave is

$$P_r = \frac{1}{2\eta_o}\int_0^{2\pi}\int_0^{\pi/2}(|E_\theta|^2 + |E_\phi|^2) r^2 \sin\theta d\theta d\phi \tag{22}$$

the stored electric energy is

$$W_e = \frac{\varepsilon_o \varepsilon_r}{4}\iiint_{\text{cavity}} |E_z|^2 dV. \tag{23}$$

The calculation of δ_e in (21) requires an iterative procedure. It is found that the final value of δ_e is quite sensitive to the value chosen at the start of the iterative process [11]. We begin by setting $\delta_e = \delta_0$ instead of usual δ to shorten the iterative procedure. δ_0 is given by

$$\delta_0 = \frac{P_{r0}}{2\omega W_{e0}} + \delta + \frac{s}{t}. \tag{24}$$

where P_{r0} can be expressed as [12]

$$P_{r0} = \frac{V_d^2 A \pi^4}{20\,340}\left[(1-B)\left(1 - \frac{A}{15} + \frac{A^2}{420}\right) + \frac{B^2}{5}\left(2 - \frac{A}{7} + \frac{A^2}{189}\right)\right] \tag{25}$$

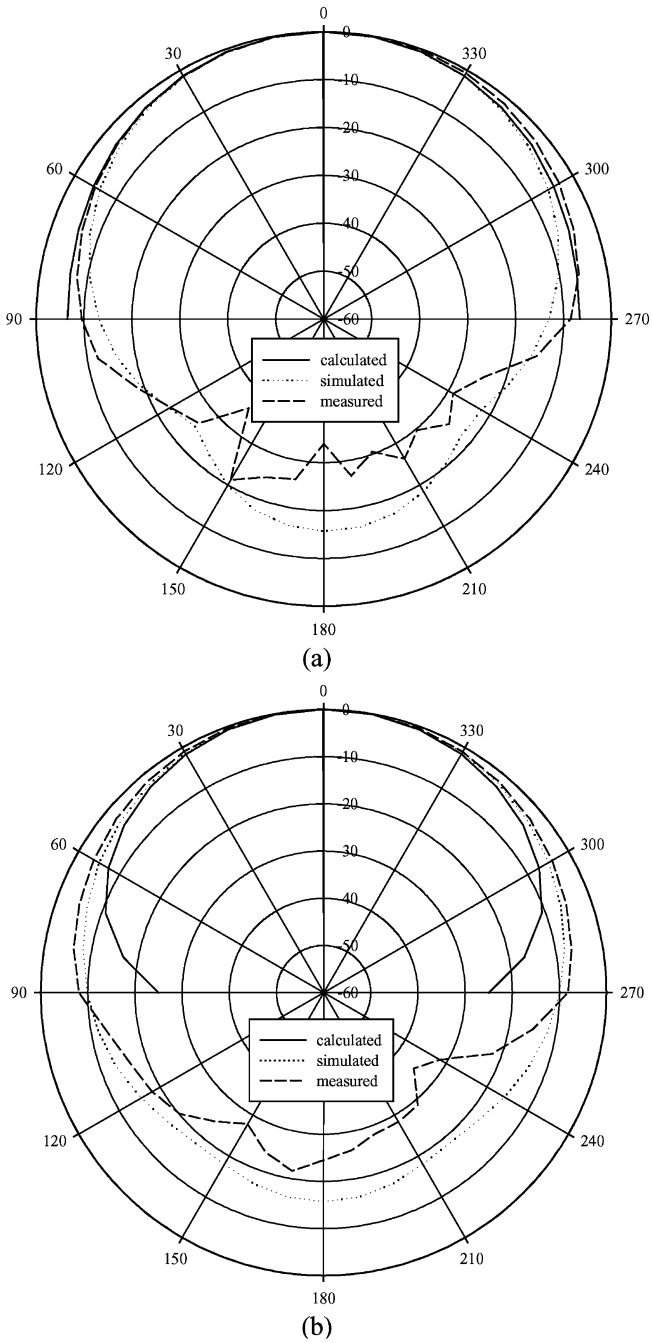

Fig. 3. Co-polar radiation patterns of the differentially-driven microstrip antenna: (a) in the E-plane and (b) in the H-plane.

with $A = (\pi a/\lambda_o)^2$ and $B = (2b/\lambda_o)^2$. There appears to be an algebraic error. Working from the approximations indicated in [12], one obtains 40 680 instead of 20 340. W_{e0}, the electric energy stored for dominant mode at resonance, can be derived to be

$$W_{e0} = \frac{\varepsilon_o \varepsilon_r a b V_d^2}{8t}. \tag{26}$$

We then calculate E_z with (16). This is followed by the calculation of $(\delta_e)_{i+1}$ with (21). The iterative process continues until the test $[(\delta_e)_{i+1} - (\delta_e)_i]/(\delta_e)_i$ is smaller than a percentage, which is usually chosen to be 2%.

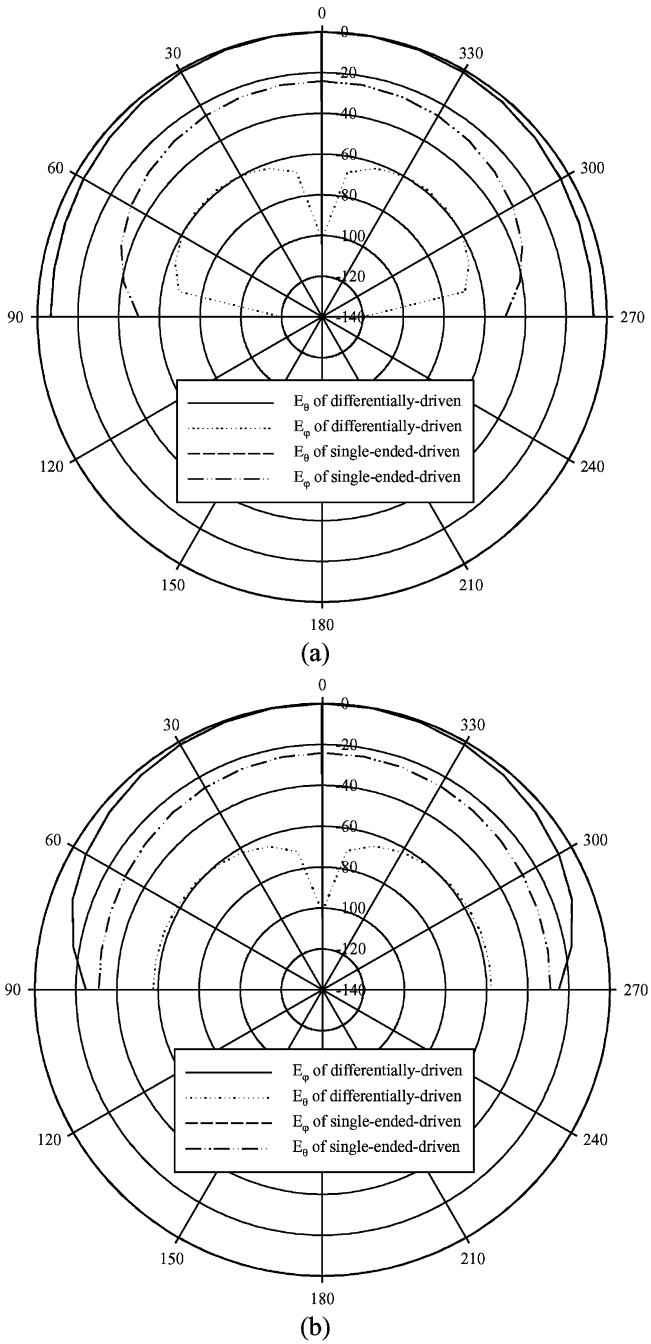

Fig. 4. Radiation patterns of the microstrip antenna for differentially-driven and single-ended-driven operations: (a) in the E-plane and (b) in the H-plane.

III. Validation of Theory of Differentially-Driven Microstrip Antennas

Theoretical calculations, numerical simulations, and physical experiments were made for a differentially-driven microstrip antenna. The antenna was constructed using Taconic TLY-5 with a relative dielectric constant of 2.2 ± 0.02 and a loss tangent of approximately 0.0009 for the substrate and a conductivity of 3.7×10^7 S/m for the conductor. It had dimensions $a = 18.522$ mm, $b = 18$ mm, and $t = 0.635$ mm. The substrate size is 25×25 mm^2. The antenna was driven differentially at both radiating edges at $(x_1, y_1) = (0.0054a, 0.5b)$ and $(x_2, y_2) = (0.9946a, 0.5b)$ to excite TM_{10} mode. This differentially-driven scheme was used in [2], [3]. The calculations were implemented in Matlab. We first calculated the effective loss tangent δ_e and then the input impedance Z_d. It was found δ_e to be 0.02 at 5.2 GHz. The simulations were executed using the HFSS. The measurements were conducted with an HP 8510C network analyzer. The measured S parameters were converted to the differential input impedance by

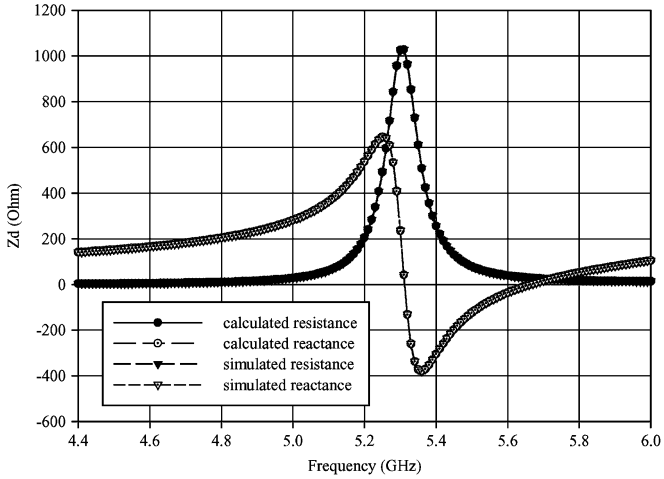

Fig. 5. Calculated and simulated differential input impedance for second driven.

$$Z_d = 2Z_o \frac{\left(1 - S_{11}^2 + S_{21}^2 - 2S_{21}\right)}{(1 - S_{11})^2 - S_{21}^2} \tag{27}$$

where Z_o is the reference impedance of 50 Ω [13].

Fig. 2 compares the calculated, simulated, and measured input impedance of the differentially-driven microstrip antenna. The impedance characteristics give insight on how the antenna must be modified to achieve a specified resonant frequency. Here the resonant frequency is defined as where the reactance of the input impedance is equal to zero. According to this definition, one can see that both calculated and simulated resonant frequencies are at 5.17 GHz and the measured resonant frequency is at 5.14 GHz. One also can see that the agreement between the calculated and simulated input impedance is excellent. The agreement between the calculated and measured input impedance is in general acceptable. The discrepancy is likely due to the fabrication tolerance and the experimental error of our measuring system. It was found that any small phase difference in measured S_{11} and S_{22} would cause a large error in the measured Z_d. It should be also noted that in any 50 Ω system, high resistance measurements are sensitive to errors.

Fig. 3 compares the calculated, simulated, and measured co-polar radiation patterns of the differentially-driven microstrip antenna at 5.25 GHz. The comparison shows that excellent agreement is obtained between the theory, simulation, and experiment in the broadside direction of the forward region. The difference in the side lobe region between the theory and simulation and experiment is because the radiation pattern is calculated for an infinite ground plane while the simulation

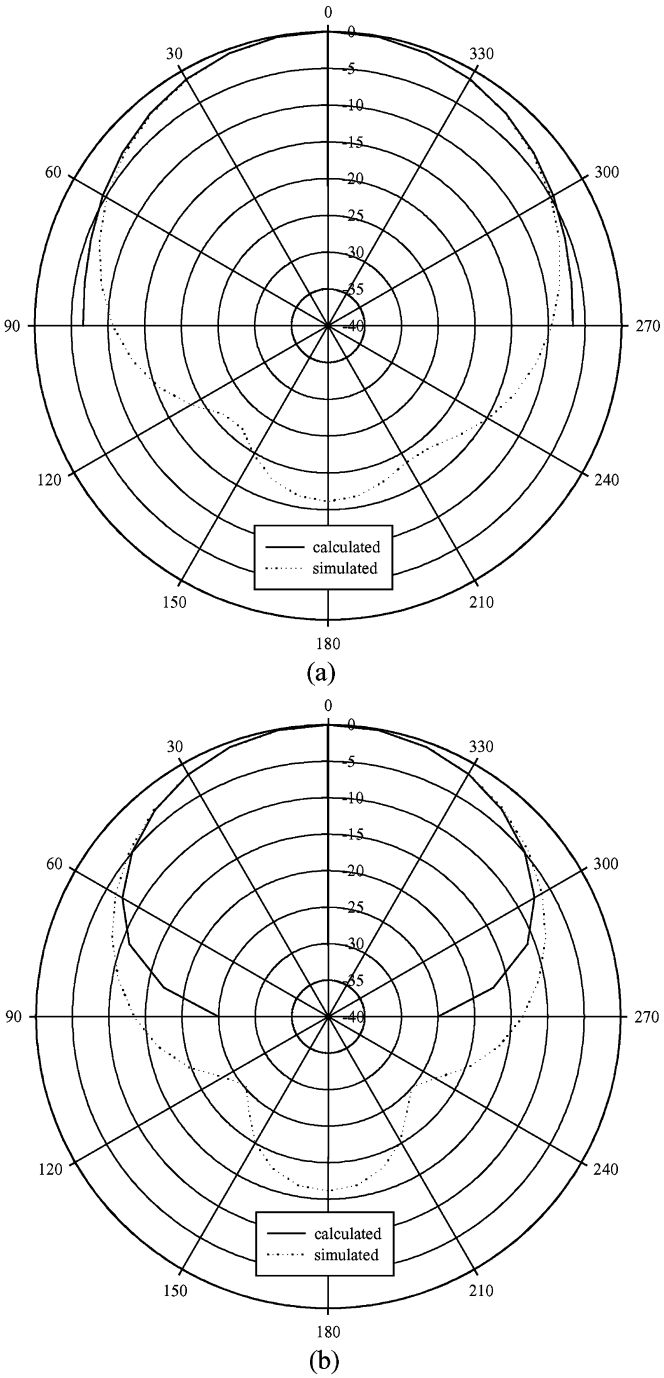

Fig. 6. Co-polar radiation patterns of the differentially-driven microstrip antenna: (a) in the E-plane and (b) in the H-plane.

and experiment are performed on a finite ground plane. We do not compare the cross-polar radiation patterns because the cross-polar radiation is quite weak and hard to measure accurately due to the cancellation mechanism introduced by the differentially-driven technique. Fig. 4 compares the calculated radiation patterns of the microstrip antenna driven for differential and single-ended operations at 5.25 GHz. It is evident from the figure that the cross-polar radiation from the differentially-driven microstrip antenna is much weaker than that of the single-ended microstrip antenna. In addition, the calculation shows that the gain of the differentially-driven

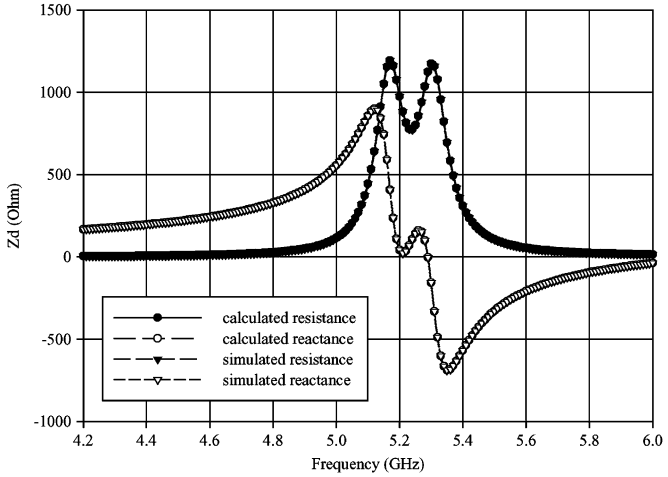

Fig. 7. Calculated and simulated differential input impedance for third driven.

microstrip antenna is almost the same as that of the single-ended microstrip antenna.

IV. Theoretcal Analysis of Differentially-Driven Microstrip Antennas

Having validated the theory, we now proceed to apply it to analyze the microstrip antenna to gain deep insight into its differential operation in this Section.

First, consider the differentially-driven points at one radiating edge: $(x_1, y_1) = (0.0054a, 0.0056b)$ and $(x_2, y_2) = (0.0054a, 0.9944b)$ to excite the TM_{01} mode. This differentially-driven scheme was used in [4]. Fig. 5 shows the calculated and simulated input impedance of the differentially-driven microstrip antenna. It is evident from the figure that the microstrip antenna resonates at 5.3 GHz and excellent agreement is obtained between the theory and simulation. Fig. 6 illustrates the calculated and simulated co-polar radiation patterns of the differentially-driven microstrip antenna at 5.45 GHz. Once again, the cross-polar radiation is negligible.

Second, consider the differentially-driven points at $(x_1, y_1) = (0.0054a, 0.0056b)$ and $(x_2, y_2) = (0.9946a, 0.9944b)$ to excite both TM_{10} and TM_{01} modes to realize circular polarization. This differentially-driven scheme has never been used. Fig. 7 shows the calculated and simulated input impedance of the differentially-driven microstrip antenna. It is evident from the figure that the microstrip antenna resonates at 5.17 GHz of the TM_{10} mode and 5.3 GHz of the TM_{01} mode and excellent agreement is obtained between the theory and simulation. Left-hand circular polarization occurs at 5.25 GHz with the minimum axial ratio of 0.5 dB in the broadside direction. The 3-dB axial ratio bandwidth is 0.96% with respect to the frequency of 5.25 GHz. Fig. 8 illustrates the calculated and simulated co-polar radiation patterns of the differentially-driven microstrip antenna at 5.25 GHz. It should be pointed out that for this case the radiation level of the cross-polar component is the same as that of the co-polar component.

As in microstrip antennas for single-ended signal operation and shown in the above three driven cases, the radiation patterns of differentially-driven microstrip antennas are not sensitive to

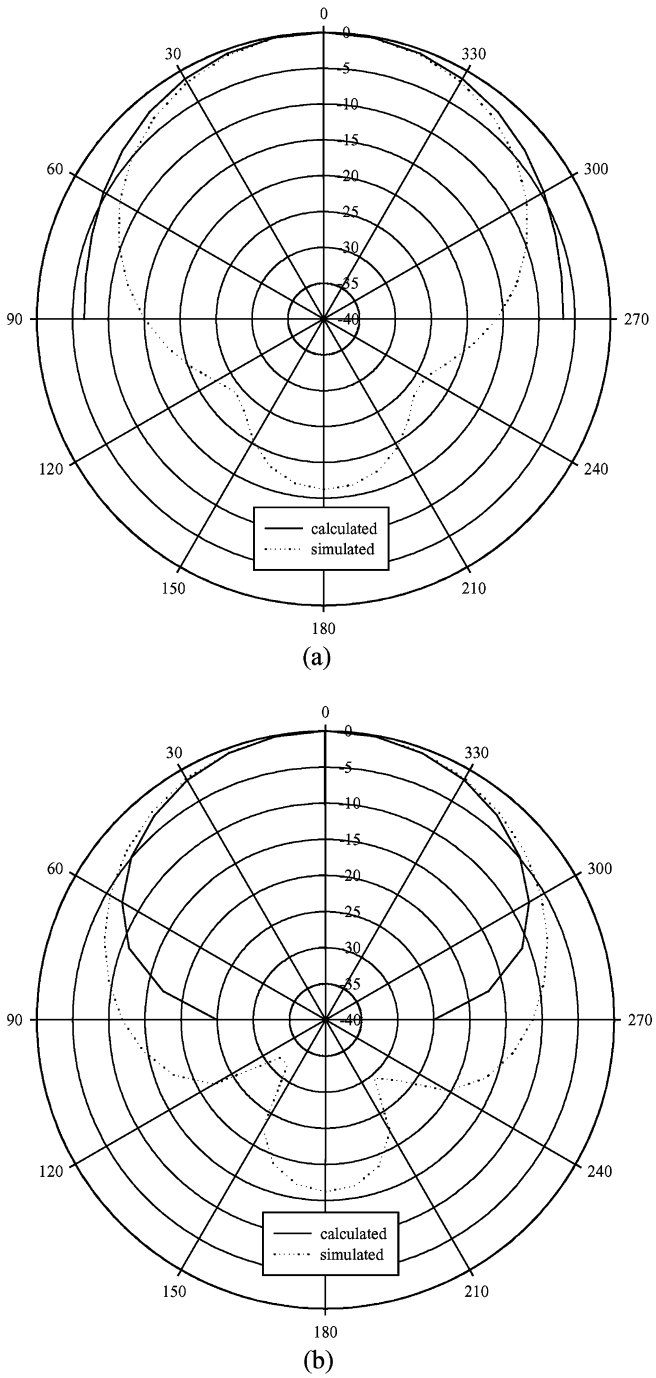

Fig. 8. Co-polar radiation patterns of the differentially-driven microstrip antenna: (a) in the E-plane and (b) in the H-plane.

the locations of the driven points. However, the physical symmetry of the locations of the driven points should be maintained for better differential performance.

Third, we analyze the differential resonant resistance as a function of ξ/λ_o for the above three differentially-driven schemes to excite the $\mathrm{TM}_{10}, \mathrm{TM}_{01}$, and both TM_{10} and TM_{01} modes, respectively. The resonant resistance for the single-ended signal operation is included for comparison. For single-ended operation, the microstrip antenna is fed at $(x_1, y_1), \xi$ is calculated with respect to a virtual feed located at (x_2, y_2). Fig. 9 shows the resonant resistance for the first

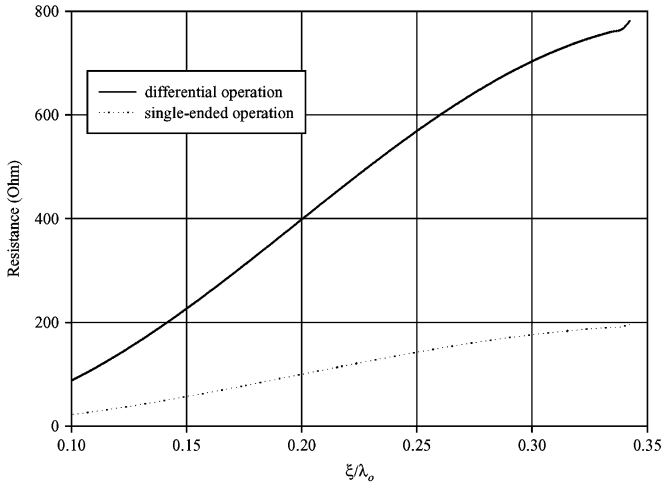

Fig. 9. Resonant resistance versus the ratio of the separation of the dual feeds to the free-space wavelength.

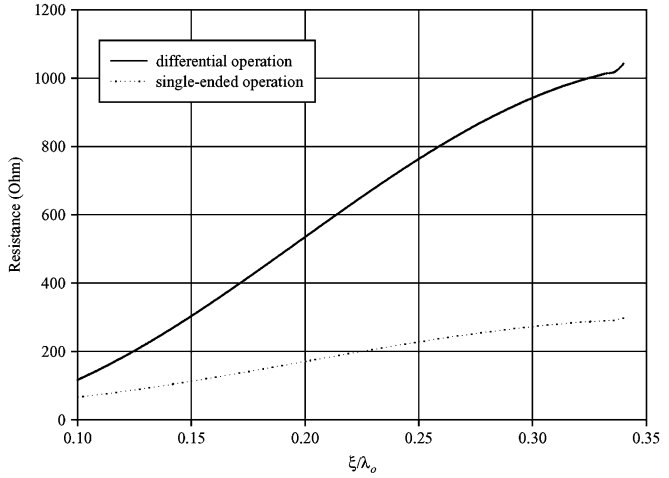

Fig. 10. Resonant resistance versus the ratio of the separation of the dual feeds to the free-space wavelength.

scheme to excite the TM_{10} mode. It is seen that the resonant resistance increase with ξ/λ_o and the differential resonant resistance is larger than the single-ended resonant resistance. It is found that when ξ/λ_o is smaller than 0.1, no resonance for differential operation will occur any more, the differential input impedance is inductive. Fig. 10 shows the resonant resistance for the second scheme to excite the TM_{01} mode. Similarly, the resonant resistance increases with ξ/λ_o and the differential resonant resistance is also larger than the single-ended resonant resistance. Fig. 11 shows the resonant resistance for the third scheme to excite the TM_{10} and TM_{01} modes for circular polarization. As can be seen from the figure, the resonant resistance increases with ξ/λ_o and the differential resonant resistance is larger than the single-ended resonant resistance. It is also found that when ξ/λ_o is smaller than 0.1, no resonance for differential operation will occur any more, the differential input impedance is inductive. The dependence of resonance for the differentially-driven microstrip antennas on the separation of the dual feeds can be explained as follows. When the dual feeds are located near to each other $\xi/\lambda_o < 0.1$, the differential

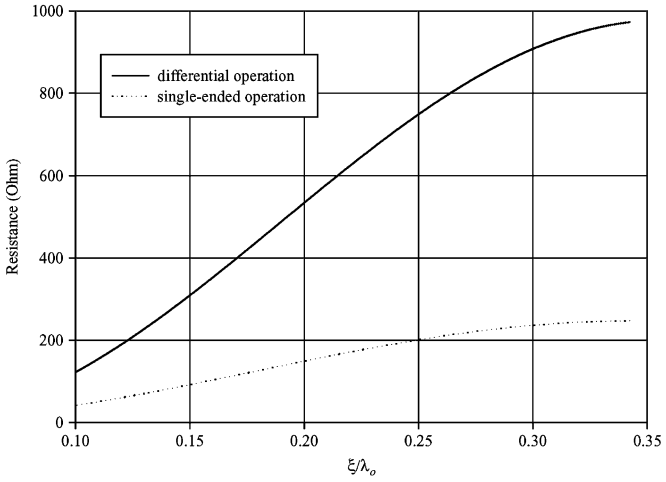

Fig. 11. Resonant resistance versus the ratio of the separation of the dual feeds to the free-space wavelength.

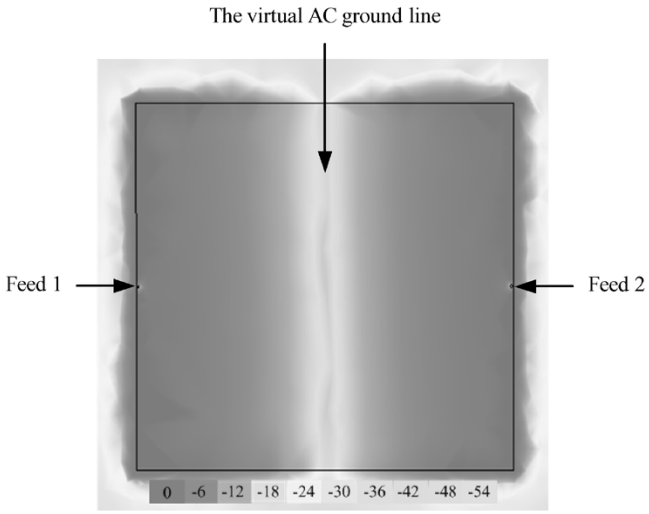

Fig. 12. Normalized E_z distribution on the surface of the differentially-driven microstrip antenna.

signal applied to the dual feeds cancels, hence the resonance does not occur and the feeds themselves make the differential input impedance exhibit inductive.

Finally, it should be mentioned that there exists a virtual ac ground line between the two feeds in the middle of the differentially-driven microstrip patch. Fig. 12 shows the normalized z component of electric field E_z in dB on the surface of the differentially-driven microstrip patch. The existence of the virtual ac ground line can be clearly identified from Fig. 12. The virtual ac ground line guarantees the isolation between the two feeds.

V. Conclusion

We have studied differentially-driven microstrip antennas theoretically and experimentally in this paper. The improved cavity model of single-ended microstrip antennas was expanded to analyze the input impedance and radiation characteristics of the differentially-driven microstrip antennas. The differentially-driven microstrip antennas were fabricated using Taconic TLY-5 and measured with the HP 8510C network analyzer. Theoretical and experimental results were found to be in acceptable agreement. It was shown from the analysis that the occurrence of resonance for the differentially-driven microstrip antennas also depends on the ratio of the separation ξ of the dual feeds to the free-space wavelength λ_o. When the dual feeds are located far from each other $\xi/\lambda_o < 0.1$, the resonance occurs, and the input resistance at resonance is rather large. However, when the dual feeds are located near to each other $\xi/\lambda_o < 0.1$, the resonance does not occur, the input resistance is quite small, and the input impedance is inductive. The comparison with single-ended microstrip antennas was made. It was found that the differentially-driven microstrip antennas have larger resonant resistance, similar co-polar radiation patterns, and lower cross-polar radiation component.

References

[1] Y. T. Lo, D. Solomon, and W. F. Richards, "Theory and experiment on microstrip antennas," *IEEE Trans. Antennas Propag.*, vol. 27, no. 2, pp. 137–145, Mar. 1979.

[2] W. R. Deal, V. Radisic, Y. X. Qian, and T. Itoh, "Integrated-antenna push-pull power amplifiers," *IEEE Trans. Microw. Theory Tech.*, vol. 47, no. 8, pp. 1418–1425, Aug. 1999.

[3] W. Wong and Y. P. Zhang, "0.18-mm CMOS push-pull power amplifier with antenna in IC package," *IEEE Microwave Wireless Comp. Lett.*, vol. 14, no. 1, pp. 13–15, 2004.

[4] P. Abele, E. Ojefors, K. B. Schad, E. Sonmez, A. Trasser, J. Konle, and H. Schumacher, "Wafer level integration of a 24 GHz differential SiGe-MMIC oscillator with a patch antenna using BCB as a dielectric layer," in *Proc. 11th GAAS Symp.*, Munich, Germany, 2003, pp. 419–422.

[5] T. Brauner, R. Vogt, and W. Bachtold, "A differential active patch antenna element for array applications," *IEEE T. Microw. Wireless Comp. Lett.*, vol. 13, no. 4, pp. 161–163, 2003.

[6] A. R. Behzad, M. S. Zhong, S. B. Anand, L. Li, K. A. Carter, M. S. Kappes, T. H. Lin, T. Nguyen, D. Yuan, S. Wu, Y. C. Wong, V. Gong, and A. Rofougaran, "A 5-GHz direct-conversion CMOS transceiver utilizing automatic frequency control for the IEEE 802.11a wireless LAN standard," *IEEE J. Solid-State Circuits*, vol. 38, no. 12, pp. 2209–2220, 2003.

[7] Y. P. Zhang, "ICPA for codesign of antenna and LNA in LTCC and CMOS,", NTU Technical Rep., 2003.

[8] W. F. Richards, Y. T. Lo, and D. D. Harrison, "An improved theory for microstrip antennas and applications," *IEEE Trans. Antennas Propag.*, vol. 29, no. 1, pp. 38–46, Jan. 1981.

[9] F. Abboud, J. P. Damiano, and A. Papiernik, "Simple model for the input impedance of coax-fed rectangular microstrip patch antenna for CAD," in *Proc. Inst. Elect.Eng. Microwaves, Antennas and Propagation*, vol. 135, 1988, pp. 323–326.

[10] J. R. James and P. S. Hall, Eds., *Characterization of Microstrip Patch Antennas and Some Methods of Improving Frequency Agility and Bandwidth*. ser. IEE Electromagnetics Waves Series. Stevenage, U.K.: Peter Peregrinus, 1989, vol. 28, ch. 3 Handbook of Microstrip Antennas. K. F. Lee, J. S. Dahele.

[11] K. F. Lee, S. R. Chebolu, W. Chen, and R. Q. Lee, "on the role of substrate loss tangent in the cavity model theory of microstrip patch antennas," *IEEE Trans. Antennas Propag.*, vol. 42, no. 1, pp. 110–112, Jan. 1994.

[12] D. Thouroude, M. Himdi, and J. P. Daniel, "CAD-oriented cavity model for rectangular patches," *IEE Electron. Lett.*, vol. 26, no. 13, pp. 842–844, 1990.

[13] R. Meys and F. Janssens, "Measuring the impedance of balanced antennas by an S-parameter method," *IEEE Antennas Propag. Mag.*, vol. 40, no. 6, pp. 62–65, 1998.

Y. P. Zhang received the B.E. and M.E. degrees from Taiyuan Polytechnic Institute and Shanxi Mining Institute of Taiyuan University of Technology, Shanxi, China, in 1982 and 1987, respectively and the Ph.D. degree from the Chinese University of Hong Kong, in 1995, all in electronic engineering.

From 1982 to 1984, he worked at Shanxi Electronic Industry Bureau, from 1990 to 1992, the University of Liverpool, Liverpool, U.K., and from 1996 to 1997, City University of Hong Kong. From 1987 to 1990, he taught at Shanxi Mining Institute and from 1997 to 1998, the University of Hong Kong. He was promoted to a Full Professor at Taiyuan University of Technology, in 1996. He is now an Associate Professor with the School of Electrical and Electronic Engineering, Nanyang Technological University, Singapore. He leads the Micro Radio Group at the Integrated Systems Research Lab to develop radio technologies for wireless communications. His research interests include propagation of radio waves, characterization of radio channels, miniaturization of antennas, design of RFICs, and implementation of wireless communications systems.

Prof. Zhang received the Sino-British Technical Collaboration Award in 1990 for his contribution to the advancement of subsurface radio science and technology. He also received the Best Paper Award from the Second International Symposium on Communication Systems, Networks and Digital Signal Processing, July 2000, Bournemouth, U.K. He is listed in *Marquis Who's Who in Science* and *Cambridge IBC 2000 Outstanding Scientists of the 21st Century*. He serves on the Editorial Board of the *International Journal of RF and Microwave Computer-Aided Engineering* and is a Guest Editor for the special issue *Journal RF and Microwave Subsystem Modules for Wireless Communications*.

J. J. Wang received the B.E. degree from Shandong University of Technology, Shandong, China, and the M.E. degree from Shanghai University, Shanghai, China, in 1999 and 2002 respectively, all in electronic engineering. She is currently working toward the Ph.D. degree at the School of Electrical and Electronic Engineering, Nanyang Technological University, Singapore.

Her research interests include microstrip antenna and radio frequency circuits design.